Variational Quantum Monte-Carlo Method in Surface Physics

W. Schattke[a], R. Bahnsen[a], and R. Redmer[b]
[a] *Institut für Theoretische Physik und Astrophysik, Universität Kiel, D–24098 Kiel, Germany* [b] *Institut für Theoretische Physik, Universität Rostock, D–18051 Rostock, Germany*

The role of the variational quantum Monte-Carlo (VMC) method for homogeneous systems and bulk material, on one hand, and finite aggregates like molecules , on the other, is now well established, mainly for the determination of ground state properties. It has been recently shown that it may be also used in surface investigations. Furthermore, dynamic behavior seems to be accessible, too, in view of the numerical resolution currently achieved. This applies also to surface dynamics. Considering the still smaller energy scales as represented by the electron-phonon interaction represents the actual borderline of accessible resolution. Nevertheless, localized electronic excitations could be investigated in bulk solids in order to yield the changes in excitation energy induced by a deformation, which shows thus a possible access to the deformation potentials.

1 Introduction

Since the first principal steps which were mainly devoted to homogeneous systems [1, 2] quantum Monte-Carlo (QMC) methods have steadily evolved with respect to the techniques as well as to the extent of application. For a recent review and references therein see Foulkes et al.. [3]

One branch, being that we treat in this article, is based on the use of the quantum mechanical wave function in the form of a parametrized variational *ansatz*. Ritz's variational principle is applied to find the best parameter fit. Frequently, further treatment proceeds via numerical relaxation through a diffusion-like equation, called diffusion Monte-Carlo (DMC). A lower energy and better approximation of the wave function is obtained, but as a draw back it is more demanding from both human and computational ressources, it is less illustrative and it yields the wave function only in numerical form, i.e. more cumbersome for calculations of derived quantities. For the first steps of QMC into a new field, as it is described here, VMC deserves its own right of application which has been demonstrated many times in the past.

Among the goals QMC has achieved in the early times the most important for *ab-initio* studies of material science was the determination of the exchange-correlation functional for density functional theory. [4, 5, 6] To this end, the ground state energy was calculated for the homogeneous electron gas via QMC as a function of density. Within local density approximation (LDA) the result has been locally transferred to the density of the non-homogeneous material, e.g. of the solid. Thus, from a principal point of view direct application of QMC to non-homogeneous systems could generally serve to find an improved density functional which is better adapted to some class of materials than present extensions of LDA. [7]

Of course, direct investigations of specific systems with QMC make sense as prototype estimates of the accuracy of usual *ab-initio* methods, because the error in the QMC calculation can be safely recorded by statistical methods. In addition, they are predictive

for the material at hand. Such applications to solids aim at the ground state geometry with its structural parameters, at the total energy, at the cohesive energy, at the bulk modulus, at the electron density, and at the electron density correlation function, to name the main quantities.

Other topics of solids, not yet standard as the afore mentioned ones, are e.g. excited states of the bulk where first successful investigation have already been achieved. [8] Applications to phonon dynamics and to the field of solid surfaces, disregarding here cluster systems, are still missing. It is the aim of this work to show that these topics are within the reach of QMC. For definiteness, the used VMC method will be outlined with the specific details which requires also the presentation of some basic notions.

2 Variational quantum Monte-Carlo

2.1 General method

Variational quantum Monte-Carlo is based on Ritz's variational principle and minimizes the expectation value of the exact hamiltonian of an N-particle quantum system with respect to chosen variational parameters of the ansatz for the N-particle wave function. This ansatz generally is the better the lower the energy appears provided the integration for the expectation value is exact. The latter is done by Monte-Carlo integration and bears a statistical property whose accuracy can be controlled to arbitrary order, however. So, the success of the method depends solely on the choice of the wave function ansatz. To this end, the Jastrow-Slater form has been proved over a long period of experience to present an extremely comfortable and reliable ansatz. Though we do not know how far we are from the unknown exact ground state energy, a relative improvement of the wave function is safely recorded by a lowering of the energy expectation value and in addition, an absolute measure of its accuracy is provided by the variance of that energy. No uncontrolled approximations which are quite typical in many-body theory are hidden in this method. On the contrary, the method serves to estimate the quality of those approximations.

The expectation value of the hamiltonian of a quantum system in the state Ψ_λ

$$E_\lambda = \langle \hat{H} \rangle \quad = \quad \int \frac{\left|\Psi_\lambda(\vec{Y})\right|^2}{\int \left|\Psi_\lambda(\vec{Y}')\right|^2 d\vec{Y}'} \frac{\hat{H}(\vec{Y})\Psi_\lambda(\vec{Y})}{\Psi_\lambda(\vec{Y})}\, d\vec{Y} \tag{1}$$

is written as an integration over a probability density given by the normalized wave function being multiplied by a fluctuating quantity which would be the exact energy constant in the case of an exact wave function. The amount of fluctuations reflects the error present in the wave function.

The integral is calculated by stochastic integration over the coordinates $\vec{Y} = (\vec{r}_1 s_1, ..., \vec{r}_N s_N)$ of the system, i.e. the $3N$ position variables with fixed spin of N particles which may at present easily exceed 1000. That figure shows also the inadequacy of conventional integration methods. The index vector $\vec{\lambda}$ denotes a set of parameters representing the variational freedom in the trial wave function and comprises up to several tens of different quantities each capable of a whole set of values which are to be minimized. In practice the Metropolis algorithm [9] is used to guarantee importance sampling during the random walk so that the energy can be estimated safely as the mean of the local energy with

purely statistical error

$$E_\lambda \approx \tilde{E}_\lambda := \frac{1}{M}\sum_{i=1}^{M}\frac{\hat{H}(\vec{Y}_i)\Psi_\lambda(\vec{Y}_i)}{\Psi_\lambda(\vec{Y}_i)}\,, \tag{2}$$

$$\sigma(E_\lambda) = \sqrt{\frac{1}{M}\mathrm{Var}(\frac{\hat{H}\Psi_\lambda}{\Psi_\lambda})}\,. \tag{3}$$

Thus, Ritz's variational principle ensures that the minimum $\tilde{E}_{\lambda^*}$ of $\tilde{E}_\lambda$ in the parameter space is an upper bound for the true ground state energy E_0.

The random walk over the integration points is generated by a transition probability $P(\vec{Y}_i \to \vec{Y}_{i+1})$ from configuration $\vec{Y}_i$ to configuration $\vec{Y}_{i+1}$ which is chosen to fulfil detailed balance in a stationary Markov process with the stationary probability densities given by the wave function, i.e.

$$P(\vec{Y}_i \to \vec{Y}_{i+1})|\Psi(\vec{Y}_i)|^2 - P(\vec{Y}_{i+1} \to \vec{Y}_i)|\Psi(\vec{Y}_{i+1})|^2 = 0 \tag{4}$$

This is fulfilled by

$$P(\vec{Y}_i \to \vec{Y}_{i+1}) = min(1, \frac{|\Psi(\vec{Y}_{i+1})|^2}{|\Psi(\vec{Y}_i)|^2}) \tag{5}$$

because each configuration change yields either less equal or greater then 1 for the ratio appearing in (5) which leads to the vanishing of equation 4. This choice characterizes the so-called Metropolis algorithm. [9] A total number of M such steps has been accumulated in equation 2.

In practice, one step touches in turn each single electron and accepts a randomly chosen move if a randomly chosen number from the interval $[0, 1]$ does not exceed the value in 5. The sum over the realized configurations is used in 2. As each step can be seen as the realization of an independent random variable which obeys the same distribution given by the wave function, the central limit theorem assures convergence of the sum to the integral for $M \to \infty$, if the individual variance exists. In other words, the Markov chain samples the correct configurational average. The variance of the hamiltonian $\langle(\hat{H} - < \hat{H} >)^2\rangle$ vanishes for an eigenfunction and may be used as a measure of deviation from the exact solution. From a chain of independent realizations that variance might be expected to asymptotically behave as M, i.e. the relative error would vanish according to $\frac{1}{\sqrt{M}}$, but this is multiplied by the variance of the normalized sum which might become small or large depending on the quality of the wave function. So less can be said with respect to the variance from purely statistical reasoning.

Some caution is required at the zeros of the wave function in equation 2. Although the weight vanishes there thus avoiding those configurations, the denominator may become small and enhance the variance. This occurs specifically at points where Pauli's exclusion principle forces the wave function to zero, i.e. not only if two particles of equal spin approach but always if two single particle wave functions in a Slater determinant happen to get equal values. However, these situations are realized with rapidly decreasing measure for an increasing number of electrons in the run, because of an exponential peaking of the distribution near the most probable configurations.

2.2 Hamiltonian

The hamiltonian of the considered system, here electrons in a solid or solid surface in the Born-Oppenheimer approximation, consists of the kinetic energy operator $\hat{T}$ of the electrons and the potential energy operator $\hat{V}$ of all the Coulomb interactions in the system.

The kinetic energy needs the calculation of $-\frac{1}{2}\frac{\Delta\Psi}{\Psi}$ which implies the knowledge of the wave function ansatz and will be discussed later. Green's relation shows its equivalence with $\frac{1}{2}|\frac{\nabla\Psi}{\Psi}|^2$ as an integrated property if boundary terms vanish e.g. in the case of periodic solids. By comparing the two expressions for the kinetic energy it is possible to check the numerical accuracy of the calculation. Frequently, the second derivative form showed larger fluctuations than the positive definite latter form. Nevertheless, the former expression is retained in the simulation, because this expression appears in the Schrödinger equation whose fulfilment is tested by minimization and estimation of variance.

Only for solids of light elements as e.g. Li [10] all electron calculations are allowed by present days computing power. For solids of non-light elements the inner shell electrons together with the nucleus have to be replaced by some pseudo-ion with effective charge Z' and a nonlocal electron-ion pseudopotential for the valence electrons. [11] This is still a crucial point which might spoil the accuracy, though it is inherent in the respective density functional calculations, too. It is not yet clear whether special forms of pseudopotentials are superior here, so that those forms basing on reference [12] and widely used in the local density approximation (LDA) are applied. However, one might expect that especially quantities as the cohesive energy which need a comparison between an atomic and a bulk quantity may be influenced by the inadequacy of the pseudopotential to either of these systems.

Now, the potential energy operator reads

$$\hat{V} = \hat{V}_C + \hat{V}_{PP}^{\mathrm{l}} + \hat{V}_{PP}^{\mathrm{nl}} \ , \tag{6}$$

where $\hat{V}_C$ is the operator of the remaining Coulomb interactions and $\hat{V}_{PP}^{\mathrm{l}}$ and $\hat{V}_{PP}^{\mathrm{nl}}$ are the local resp. nonlocal parts of the pseudopotential. The nonlocal part is evaluated in a semilocal form, see e.g. [11, 13].

$$\hat{V}_{PP}^{\mathrm{nl}}(\vec{r}) = \sum_{l=0}^{\infty} V_l(r)|l><l|, \tag{7}$$

$$|l><l| = \sum_{m=-l}^{l} Y_{lm}(\vec{r}) \int_{r'=r} d\vec{r}' Y_{lm}(\vec{r}') \tag{8}$$

$$= Y_{l0}(\vec{z}) \int_{r'=r} d\vec{r}' Y_{l0}(\vec{r}') \ , \tag{9}$$

the latter if the z-axis is locally aligned with $\vec{r}$. The projector contains an angle integration over the sphere which is discretized according to the number of angular momenta which approximately constitute the decomposition of unity in the relevant Hilbert space of the system. For GaAs this has been proved to occur already for the set $l = 0, 1$ which yields a number of 4 angles to be summed over. The calculation of the potential, especially the nonlocal part, appears to be rather tedious when performed within a simulation step. Trials to use smaller numbers of simulation points for parts of the potentials have proved to fail, if the wave function differs from being an eigenfunction in some essential regions

as e.g. in the neighborhood of nuclei. As a consequence, all these terms are conveniently precalculated, tabulated, and interpolated.

The resulting Coulomb energy-like operator collects together the constant ion-ion-energy, some part of the electron-ion interaction, and the full electron-electron interaction

$$\hat{V}_C = E_{ii} + \hat{V}_{ei} + \hat{V}_{ee} \ , \tag{10}$$

thereby including the contributions of the Z'/r-asymptotics of $\hat{V}_{PP}^{\rm l}$ among $\hat{V}_{ei}$. The remaining pseudopotential part is short ranged, and only $\hat{V}_C$ is affected by the boundary conditions. To account e.g. for periodic boundary conditions, a superlattice with vectors $\{\vec{R}^i\}$ is introduced, which adds to an arbitrary position of charge its periodic counterparts.

2.3 Wave Function

The success of a variational procedure depends on the quality of the variational space spanned by the admitted wave functions. In comparison to quantum chemical methods the successful application of VMC to atoms, clusters, pure solids and those with imperfections is mainly due to the finding of compact forms for the many-body wave function which allow a comfortable scaling with particle number, i.e. system size. The *ansatz* most widely used in VMC is the Slater-Jastrow type $\Psi = \Psi_S \Psi_J$ which consists of the product of two Slater determinants Ψ_S, for each of both spin directions one determinant for the singlet ground state, and the symmetrical Jastrow factor Ψ_J.

$$\begin{aligned} \Psi(\vec{r}_1\sigma_1, \ldots, \vec{r}_N\sigma_N) &= D^{\uparrow}(\vec{r}_1, \ldots, \vec{r}_{N/2}) D^{\downarrow}(\vec{r}_{N/2+1}, \ldots, \vec{r}_N) \\ &\times \exp\Big[-\sum_{i<j} u(\vec{r}_{ij}, \sigma_{ij}) \Big] . \end{aligned} \tag{11}$$

The two-particle expression in the exponent depends on σ_{ij} which denotes the two possibilities of both spins i, j to be parallel or antiparallel. Some forms of this expression have been discussed in the literature [3] leaving more or less as a standard

$$u(\vec{r}, \sigma) = A\Big[\frac{1}{r} + v^b(\vec{r}\,)\Big] \Big(1 - e^{-r/F(\sigma)}\Big) \ . \tag{12}$$

Disregarding for a moment v^b the expression 12 which vanishes for large distance r between both particles reduces the wave function for decreasing distance reflecting the Coulombic repulsion. The parameters A, F are chosen such that in the total energy the Coulomb and all other $\frac{1}{r}$ terms are cancelled for $r \to 0$, the so-called *cusp condition*. In the solid one must take care of the boundary condition that corresponds to exactly periodically repeating the values of the wave function onto the lattice given by the simulation cell. That is achieved by adding a full Ewald summation to u which is included within the square brackets via v^b because only the long range $\frac{1}{r}$ part changes for reasonably large simulation cells. Occasionally, a one-particle function is added in the exponent of the Jastrow factor in order to adjust the determinantal part of the wave function for an exaggerate spread of the electron density by the interelectronic Jastrow repulsion. [11, 14] In the case that analytical expressions for variational single particle waves in the determinant are available such an adjustment is not necessary. However, we will see later how this can be utilized to describe a finite slab system.

For the single particle waves $\phi_i(\vec{r}_k)$ as elements in the determinant D_{ik}, numerical results from precursor density functional calculations may be used as well as analytical forms with additional variational parameters. The latter are flexible and computationally easy. The use of single plane waves showed to be inferior to localized functions even in a metal like Lithium. [10] Localized orbitals are conveniently used, bare or hybridized to account for directed bonds and molecular linear combinations in semiconductors.

2.4 Update of Wave Function

For the probability in the Metropolis algorithm the ratio between the new Ψ^{new} and old wave function Ψ^{old} is needed

$$\frac{\Psi^{new}}{\Psi^{old}} = \frac{\Psi_S^{new}}{\Psi_S^{old}} \frac{\Psi_J^{new}}{\Psi_J^{old}} \tag{13}$$

where the ratio of the Jastrow factors is evident and for the ratio of the determinants $det(D)$ the cofactors $\bar{D}_{lm}$ with

$$1 = \sum_i \phi_i(\vec{r}_k)\bar{D}_{ik} \tag{14}$$

$$\frac{\Psi_S^{new}}{\Psi_S^{old}} = \sum_i \phi_i(\vec{r}_k^{new})\bar{D}_{ik}^{old} =: q \tag{15}$$

are used via the Sherman-Morrison-Woodbury lemma to determine the update of cofactors. Denote a kth column vector for the change of determinants $v := D_{.k}^{new} - D_{.k}^{old}$ and the kth unit vector e then the matrix identity

$$(D + ve^T)^{-1} = D^{-1} - \frac{D^{-1}ve^TD^{-1}}{1 + e^TD^{-1}v} \tag{16}$$

yields with q from 15

$$\bar{D}_{lm}^{new} = \frac{1}{q}\bar{D}_{lm}^{old} \qquad \text{for} \quad m = k \tag{17}$$

$$= \bar{D}_{lm}^{old} - \frac{1}{q}\bar{D}_{lk}^{old} \sum_i \bar{D}_{im}^{old} D_{ik}^{new} \qquad \text{for} \quad m \neq k. \tag{18}$$

As in 14, also in the kinetic energy terms only the cofactors appear such that the value of the determinant which varies over orders of magnitude within a run has never to be calculated.

$$\frac{\Delta_k\Psi}{\Psi} = \frac{\Delta_k\Psi_S}{\Psi_S} + \frac{\Delta_k\Psi_J}{\Psi_J} + 2\frac{\vec{\nabla}_k\Psi_S}{\Psi_S}\frac{\vec{\nabla}_k\Psi_J}{\Psi_J} \tag{19}$$

$$\frac{\vec{\nabla}_k\Psi_S}{\Psi_S} = \sum_i \vec{\nabla}_k\phi_i(\vec{r}_k)\bar{D}_{ik} \tag{20}$$

$$\frac{\Delta_k\Psi_S}{\Psi_S} = \sum_i \Delta_k\phi_i(\vec{r}_k)\bar{D}_{ik} \tag{21}$$

At this stage, we can note the shape of the cusp condition. Because of antisymmetry the wave function vanishes as

$$\Psi_S = \vec{r}_{lm}\vec{\nabla}_l\Psi_S \tag{22}$$

with the difference vector $\vec{r}_{lm}$. The kinetic energy of the Jastrow factor contains according to 22 and 19

$$\lim_{r_{lm}\to 0} 2\left(\frac{\vec{\nabla}_l\Psi_S}{\Psi_S}\frac{\vec{\nabla}_l\Psi_J}{\Psi_J} + \frac{\vec{\nabla}_m\Psi_S}{\Psi_S}\frac{\vec{\nabla}_m\Psi_J}{\Psi_J}\right) = -\frac{4}{r_{lm}}\frac{du}{dr_{lm}}\delta_{s_l s_m} \tag{23}$$

In atomic units, this part and $\frac{\Delta_k\Psi_J}{\Psi_J}$ both multiplied by $-\frac{1}{2}$ plus the Coulomb $\frac{1}{r}$ part yield

$$\lim_{r\to 0}\left[\frac{1}{r} + \left(\Delta u - \left(\frac{du}{dr}\right)^2 + \frac{2}{r}\frac{du}{dr}\delta_{s_l s_m}\right)\right] \tag{24}$$

where the $\frac{1}{r}$ coefficient should cancel leaving a constant in this limit. Viewed as an equation for $\frac{du}{dr}$ expression 24 shows immediately that

$$\frac{du}{dr}|_{r=0} = -\frac{1}{2} \qquad \text{for} \quad s_l \neq s_m \tag{25}$$

$$= -\frac{1}{4} \qquad \text{for} \quad s_l = s_m \tag{26}$$

has to be fulfilled if the second derivative of u with respect to r is required to be finite. This is a condition for the parameters in the Jastrow exponent.

2.5 Optimization

The energy has to be a minimum and the variance has to vanish for an eigenstate. Both constitute a criterion to estimate the wave function as a function of its parameters and it actually seems to be a question of strategic preference which to apply, because the whole task, sampling and minimization, is a rather detailed sequence of single acts. A lot of calculations base on *correlated sampling*, i.e. one generates a set of configurations from a fixed distribution and minimizes the variance with respect to the wave function parameters. The configuration set is regenerated utilizing the optimum parameter values and iterated to convergence. Using the same distribution for different parameter values may also be an aim to sample local differences in order to compare quantities whose global sums become too inaccurate. Within correlated sampling variance minimization is favored in comparison with energy minimization. Tests on noninteracting systems have shown that the stability at small values of the wave function occurring near the nodal surfaces and the finite sampling is better for variance minimization. [15, 16, 17, 18, 19, 20]

Here, we use the alternative to generate uncorrelated sets of configurations for each choice of the parameter vector and record energy expectation value and variance together. Minimization of the expectation value is performed by statistical regression and followed by a sampling with long runs near the minimum. The one-particle functions in the Slater determinant contain variational freedom, too, so that a shift of the nodal surface may occur and is considered as a variational advantage. Furthermore, these functions adjust for the enhanced repulsion by the Jastrow factor and a special one-particle term in the Jastrow factor for that reason is avoided. The energy landscape appears to be rather smooth and more advanced methods of global minimization as simulated annealing or genetic algorithms are not needed.

In a parabolic mean square regression of order 2 of the quantum mechanical expectation value E as a random variable with respect to the random variable represented by

the m-dimensional parameter vector $\vec{\lambda}$ the normalized mean square deviation

$$\chi^2 = \sum_{i=1}^{l} \frac{(E_i - f(\vec{\lambda}_i))^2}{\Delta^2 E_i} \tag{27}$$

$$= (\vec{E} - F\vec{a})^T W (\vec{E} - F\vec{a}) \tag{28}$$

is minimized to find the functional dependence in form of a sum of order $n \leq 2$ polynomials

$$f(\vec{\lambda}) = \sum_{j=1}^{p} a_j \, p_j(\vec{\lambda}) \tag{29}$$

with linear coefficients collected into a p-dimensional vector $\vec{a} = (a_1, ..., a_p)$. Equation 28 condenses 27 into vector form with diagonal matrix W of reciprocal variances and F to be the $(l \times p)$ matrix $F_{ij} = p_j(\vec{\lambda}_i)$ Order 2 is chosen because near the minimum the energy should be reasonably represented by a quadratic form in $\vec{\lambda}$, i.e.

$$E(\vec{\lambda}) = A_0 + \vec{b}^T \cdot \vec{\lambda} + \vec{\lambda}^T \, A \, \vec{\lambda} \tag{30}$$

with $(m \times m)$ matrix A positive definite because of the energy being bounded from below. The determination of $\vec{a}$ follows from the minimum of equation 28 by solution of a linear system provided the number of parameter values $l > p$ is sufficient such that the $(p \times p)$ matrix $(F^T W F)$ is non-singular. It yields

$$\vec{a} = (F^T W F)^{-1} \, F^T \, W \, \vec{E} \tag{31}$$

$$V[\vec{a}] = (F^T W F)^{-1} \tag{32}$$

the mean together with the covariance matrix V. The diagonal elements of the latter give by their square roots the 'best' estimate for the standard deviations of $\vec{a}$.

After fixing the fitting coefficients $\vec{a}$ for the quadratic polynomial decomposition of the energy 30, we obtain by minimization with respect to the $\vec{\lambda}$ the estimate of the parameter values in the wave function and of the ground state energy, viz.

$$\frac{\partial E(\vec{\lambda})}{\partial \vec{\lambda}} = 0 \tag{33}$$

and

$$\vec{\lambda}^*(\vec{a}) = -\frac{1}{2} A^{-1}(\vec{a}) \, \vec{b}(\vec{a}) \tag{34}$$

$$E^*(\vec{a}) = A_0 - \frac{1}{4} \vec{b}^T(\vec{a}) \, A^{-1}(\vec{a}) \, \vec{b}(\vec{a}) \, . \tag{35}$$

The determination of the covariance matrices of the above quantities and a possible representation of the polynomials are summarized in appendix A.

3 Bulk Solids

3.1 Ground State

The central point in VMC calculations for the solid compared to finite systems are the boundary conditions. The sampling is done in the simulation cell with volume Ω which

comprises a certain number of unit cells. We use a notation $(l \times m \times n)$ to denote these numbers along the crystal axes. These numbers can be only rather small by computational limitations and a suitable boundary condition which simulates a larger effective volume has to be implemented. This condition uses an exact periodic repetition of the simulation cell in all three space directions so as to render the observables as well as the wave function completely periodic. The wave function is not periodic under translation of a single electronic position and the condition corresponds to the neglect of the individual Bloch phases in a single particle picture which is the essential error made in describing an infinitely extended solid. In order that the simulation itself, i.e. the random walk, shows this periodicity, each step leaving the simulation cell must enter this cell at a periodically equivalent site. This has to be explicitly programmed.

Furthermore, two-body expressions in the wave function and the potential have to be periodic which is achieved by Ewald sums. The determination within run time would by far surpass the computational resources. Thus, these expressions have to be precalculated and tabulated.

To be concrete consider e.g. the Coulomb potential. The same applies to the exponent of the Jastrow factor as a two-body expression. However, the position variable of the particle actually sampled becomes periodic by backfolding into the simulation cell and so does a one-body potential and each single particle function in the Slater determinant. Thus, the total Coulomb interaction reads

$$\begin{aligned} 2V_C \;:=\; & \sum_i \left[\sum_{j \neq i} \left(\sum_\nu \frac{1}{|\vec{r}_i - \vec{r}_j - \vec{R}_\nu|} \right) + \sum_{\nu \neq 0} \frac{1}{|\vec{R}_\nu|} \right] \\ & -2 \sum_i \sum_\alpha \sum_\nu \frac{Z_\alpha}{|\vec{r}_i - \vec{R}_\alpha - \vec{R}_\nu|} \\ & + \sum_\alpha \left[\sum_{\alpha' \neq \alpha} \left(\sum_\nu \frac{Z_\alpha Z_{\alpha'}}{|\vec{R}_\alpha - \vec{R}_{\alpha'} - \vec{R}_\nu|} \right) + \sum_{\nu \neq 0} \frac{Z_\alpha^2}{|\vec{R}_\nu|} \right] . \end{aligned} \tag{36}$$

Indices α and i run over the nuclei and electrons, respectively, in the simulation cell, Z_α denotes the effective atomic number of the pseudo ion, and $\vec{R}_\nu$ corresponds to the lattice vectors of the periodic repetition of the simulation cell. The summation in 36 is convergent if calculated as a whole. Splitting it needs the addition of compensating jellium terms which is, of course, well known in the three-dimensional case. It becomes tedious for the two-dimensional systems as we will see at the discussion of the surface system.

The implementation writes the two-body interaction with charges Z_γ and $Z_{\gamma'}$, defined on the simulation cell, as

$$V(\vec{r}_\gamma, \vec{r}_{\gamma'}) = Z_\gamma Z_{\gamma'} \left(\frac{1}{|\vec{r}_\gamma - \vec{r}_{\gamma'}|} + v^b(\vec{r}_\gamma - \vec{r}_{\gamma'}) \right) \tag{37}$$

with Ewald potential $v^b(\vec{r}_\gamma - \vec{r}_{\gamma'})$

$$v^b(\vec{r}) = \sum_{|\vec{R}_\nu| < R_{max}} \frac{\mathrm{erfc}(\alpha |\vec{r} - \vec{R}_\nu|)}{|\vec{r} - \vec{R}_\nu|} + \sum_{|\vec{k}| < k_{max}} V_0(\alpha, \vec{k}) \cos(\vec{k}\vec{r}) \tag{38}$$

and

$$V_0(\alpha,\vec{k}) = \frac{4\pi}{\Omega k^2}\exp(-\frac{k^2}{4\alpha^2}) \qquad \text{for} \quad k \neq 0 \tag{39}$$

$$= -\frac{\pi}{\Omega\alpha^2} \qquad \text{for} \quad k = 0. \tag{40}$$

The above expression is tabulated and applied to each type of the three interactions, $E_{ii}, \hat{V}_{ei}, \hat{V}_{ee}$, though the first one is fixed and only has to be used once.

Numerous applications determining the ground state energy and bulk modulus exist in the literature and show the reliability of the VMC method. It ranges from metals to compound semiconductors. An example is shown with figure 1 for GaAs through the dependence of total energy on lattice constant. It reflects minimum total energy, equilib-

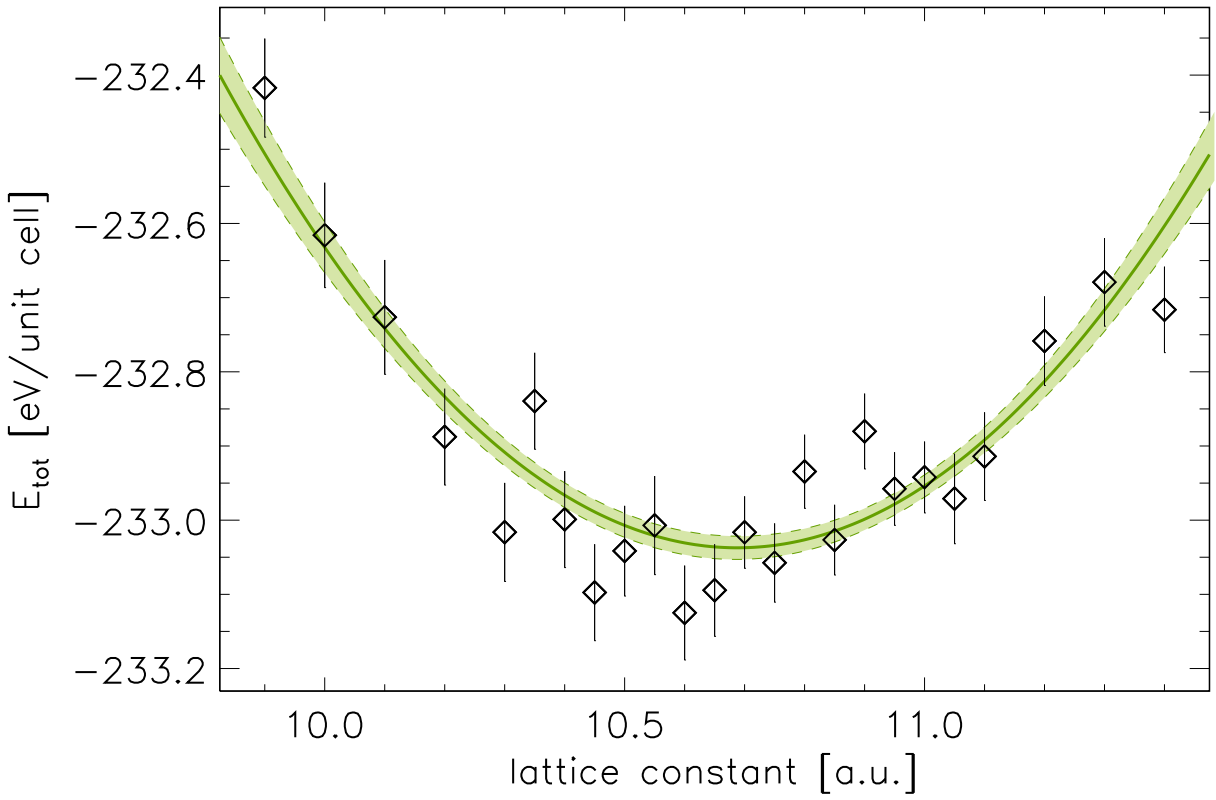

Figure 1: Total energy of GaAs vs. lattice constant.

rium lattice constant, bulk modulus, and with the knowledge of the atomic value also the cohesive energy which are collected in table 1. The close agreement with experiment is convincing. The cohesive energy of VMC in GaAs suffers probably from the pseudopotential which may be not so adapted to the atom.

	E_{atom} eV/uc	E_{tot} eV/uc	E_{bind} eV/uc	a_0 Bohr	B kbar
C (diamond) exp.	-148.02	-155.39	-7.37	6.74	4430
C (diamond) VMC [11]	-147.93	-155.38	-7.54	6.69	4200
Si exp.	-103.129	-107.97	-4.84	10.26	988
Si VMC [11]	-103.42	-108.30	-4.88	10.20	1080
Ge exp.	-103.763	-107.613	-3.85	10.678	
Ge VMC [21]	-103.23	-107.28	-4.05		
Ge DMC [21]	-103.42	-107.74	-4.32		
GaAs exp. [22]	-226.773	-233.43	-6.67	10.6831	769
GaAs VMC [13]	-228.134	-233.04	-4.9	10.689	786

Table 1: Total energy of atom, of solid, cohesive energy, lattice constant, and bulk modulus for various semiconductors, for reference to experiment see respective theoretical work

3.2 Phonon Dynamics

The ab-initio calculation of phonon spectra is already a widespread application of DFT. [23] For the VMC method this field presents a new challenge.

A parametrized variational many-body wave function with localized single particle functions offers the possibility to directly calculate the force constants from total energy. The presence of tunable parameters gives also here control over the wave function e.g. in shifting the atomic positions of the centered orbitals for a phonon displacement. The agreement of the bulk modulus with experiment shows, that with good reason, we can dispense with the full optimization and keep the parameter values of the ground state calculation. The bonding directions of the hybrid orbitals are by general construction adjusted such that they align with the direction between adjacent nuclei. A limitation occurs because of the finite size of the simulation cell which presents an upper limit for the wavelength and thus a limit for the coarseness of momentum space.

As an example, we consider the [111] phonon of GaAs at $\vec{q} = 0$. The Arsenic atoms are kept fixed and the Gallium atoms are moved along the space diagonal of the cubic unit cell. The displacement of this mode is written as

$$\vec{u}_{As} = 0, \qquad \vec{u}_{Ga} = u \frac{1}{\sqrt{3}} (\vec{e}_x + \vec{e}_y + \vec{e}_z) \tag{41}$$

with u as parameter varying from zero to up to 10 % of the lattice constant. The total energy has been calculated [24] for 51 displacements u on a (2,2,8) simulation cell. The result is displayed in figure 2. The frequency of the considered mode is calculated from the

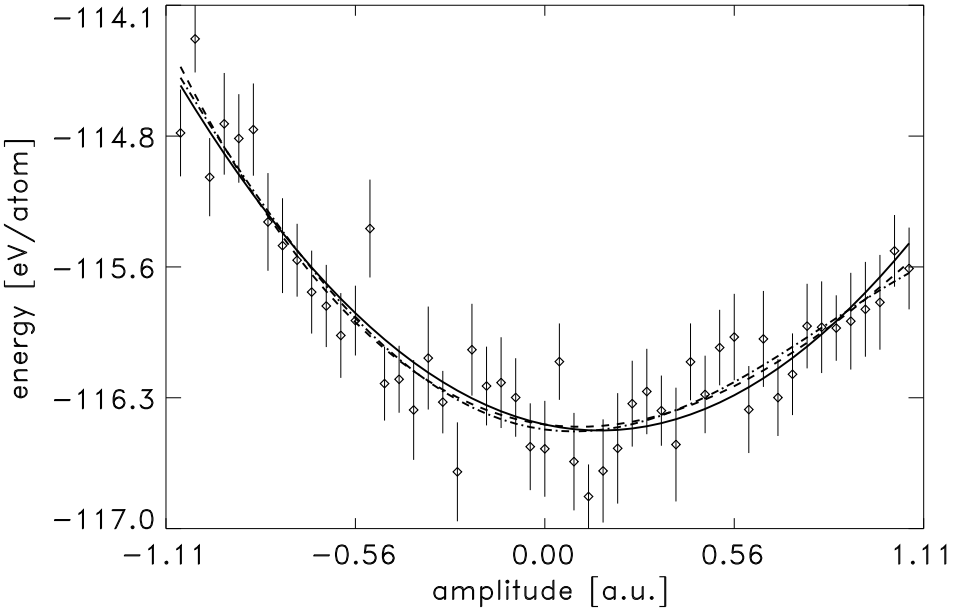

Figure 2: Total energy of GaAs vs. displacement of Ga sublattice in [111] direction for (2,2,8) simulation cell; solid, dashed, and dashed dotted line represent quadratic, cubic, and quartic regression.

quadratic coefficient and yields for various systems the results in table 2. The frequency of the 4th order anharmonic fit agrees within the attributed error, i.e. 3%, with the

experimental value of $\omega_{TO} = 33.6$ meV. [38] With respect to the splitting of the frequency by the macroscopic dipole field only the lower value applies here because the simulation cell with its periodic replication does not account long range forces. The deviation of u_{min} from zero illustrates with 0.09 a.u. the accuracy VMC achieves for a geometric determination. The test with the local pseudopotential revealed that the nonlocal version is indispensable from this respect.

3.3 Local excitation

After the success VMC has achieved with the ground state it is very tempting to extend it to the excited states. Progress in this direction is observed along the DMC method and, with some approximation, also for VMC. [25, 8, 26, 27, 28] Of course, the task is much more difficult from the computational point of view, such that in contrast to existing designs excited states cannot yet be considered as being fully accessible. Especially, the evaluation of the excitation energy as a difference from separate Monte-Carlo simulations requires extreme accuracy. The main investigations concentrate on single particle excitations as eigenvalues familiar from common bandstructures.

Here, we consider another approach, simplified because of relaxing the requirement for an eigenstate and evaluating instead a localized excitation which, of course, may contain an unknown admixture of the ground state. This would be a draw back if the lowest excitations as the band gap stand in the foreground. However, one can project onto the conduction bands and furthermore, a local excitation may deserve its own interest, as a subsequent example on the deformation potential will show.

The effect of a replacement of a specific single particle ground state orbital in the Slater determinant by a localized Gaussian with arbitrary mean and width is considered, viz.

$$\phi_{\vec{\mu},\sigma}\left(\vec{r}\right) = \frac{1}{\left(\sqrt{2\pi\sigma^2}\right)^3} \exp\left[-\frac{\left(\vec{r}-\vec{\mu}\right)^2}{2\sigma^2}\right] . \tag{42}$$

In the case of GaAs, two Arsenic hybrid orbitals, spin up and spin down, along the [111] direction at a specific As atom of the simulation cell are replaced. The total energy is recorded in figure 3 vs. the position of the Gaussian orbital along [111] for a width of $\sigma = 1.0$ a.u. for illustration. A smaller width increases the statistical variance, a

[hkl]	fit	PP	$E_{min}[eV/atom]$	$u_{min}[a.u.]$	$D[eV/a_B^2]$	$\omega[meV]$
[111]	harm.	nlok.	-116,45	0,17	5,00(06)	32,2(02)
[111]	anharm.(3.)	nlok.	-116,43	0,09	5,00(36)	32,2(12)
[111]	anharm.(4.)	nlok.	-116,46	0,09	5,93(71)	35,0(21)
[111]	harm.	lok.	-117,43	0,12	6,78(09)	37,4(02)
[111]	anharm.(3.)	lok.	-117,40	0,00	6,78(06)	37,4(02)
[111]	anharm.(4.)	lok.	-117,43	0,00	7,64(80)	39,7(21)

Table 2: Energy minimum, equilibrium position, force constant, and frequency for various fits, harmonic and anharmonic (3rd and 4th order) approximation, of a (2,2,8) GaAs system with local and nonlocal pseudopotential.

larger one loses localization. As an exception, a local pseudopotential was applied in the examples of this section. Therefore, the energy seems to drop below the bulk minimum. The lowest energy is obtained for a local excitation at the position near the center of the

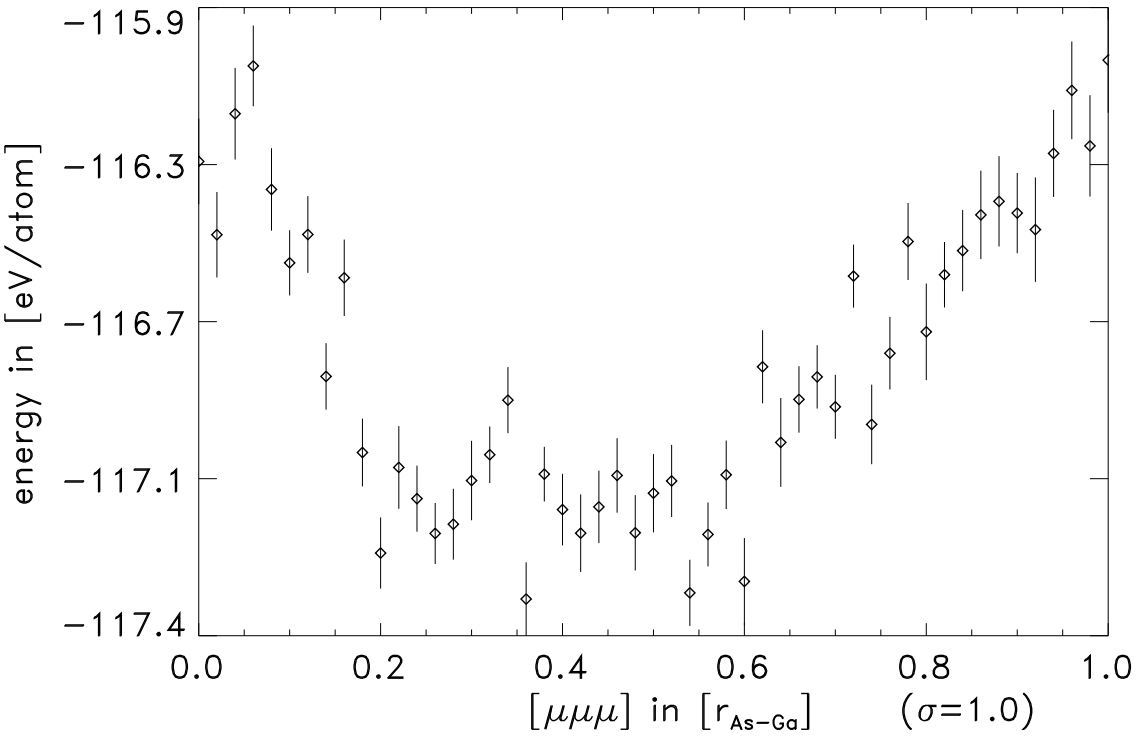

Figure 3: Total energy $E_\sigma(\vec{\mu}\,)$ vs. center $\vec{\mu}$ of excited Gaussian with $\sigma = 1.0$ for (2,2,8) system.

binding distance between As and Ga somewhat closer to Arsenic, i.e. at a position where the binding charge of the ground state orbital would be present. This confirms again the choice of the ground state single particle orbital. It shows also the energy barrier of roughly 1 eV to move both electrons away from the bonding site to the nuclei positions. This to be multiplied by the number of unit cells yielding a high value for this type of excitation. The ground state admixture should be larger at the bonding site and negligible near the nuclei.

3.4 Deformation potential

The excitations of the foregoing section serve as an estimate of the deformation potential. We consider the excitation energy as a function of a [111] optical phonon displacement $\vec{u}$ denoting by $\vec{u}_0$, $\vec{u}_-$, and $\vec{u}_+$ the equilibrium position, a decrease, and an increase (by 10 % of the lattice constant) along the cubic space diagonal of GaAs. The sampled total energies depend on the position of the excitation, also along the space diagonal, are plotted in figure 4. The shift of the maximum near $\mu = 1.0$ with the postion of the Ga atom is obvious. The deformation potential is defined as the linear displacement coefficient of the single electron band energy, or of the expectation value of the electron-phonon interaction potential. The latter may be identified with the difference between the energies plotted

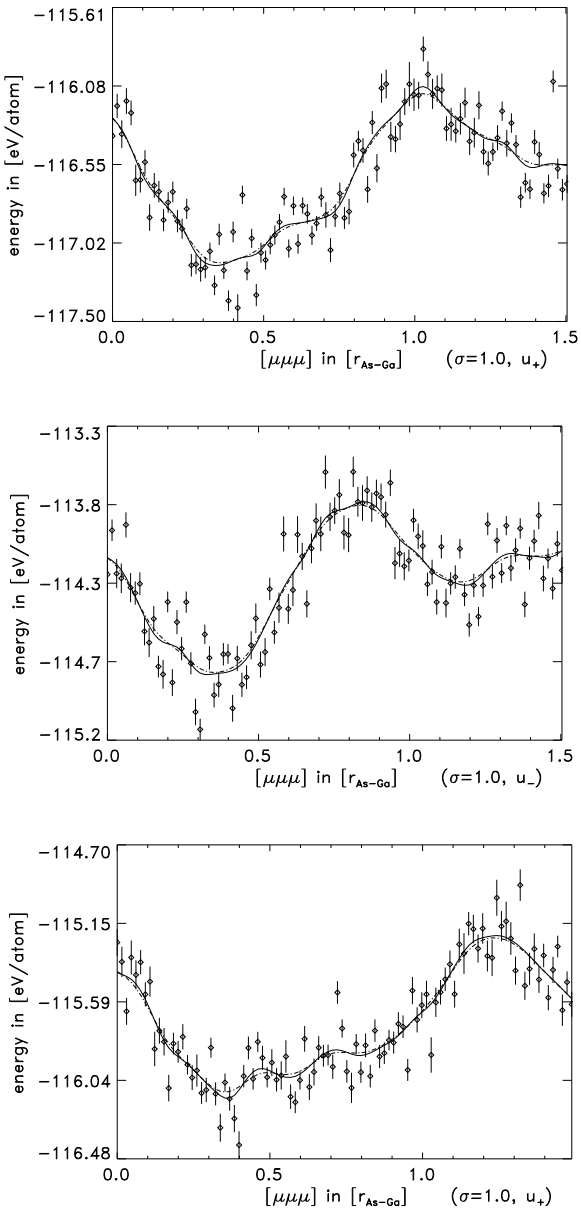

Figure 4: Total energy $E_\sigma(\vec{\mu};\vec{u})$ vs. center of Gaussian excitation with width $\sigma = 1,0$ for (2,2,8) GaAs system at equilibrium position $\vec{u}_0$ (top), with reduced Ga-As distance at $\vec{u}_-$ (middle), and with enlarged distance at $\vec{u}_+$ (bottom), solid and dashed line indicate different interpolations of data.

in figure 4 and those according to the respectively distorted ground state. Thus, we losely identify the deformation potential with

$$d_{\vec{\lambda},\vec{\xi}} = \lim_{u\to 0} \frac{\left[E(\vec{\lambda};\vec{R}_0 + u\vec{e}_{\vec{\xi}}) - E(\vec{\lambda}=0;\vec{R}_0 + u\vec{e}_{\vec{\xi}})\right] - \left[E(\vec{\lambda};\vec{R}_0) - E(\vec{\lambda}=0;\vec{R}_0)\right]}{u}. \quad (43)$$

Here, λ denotes the excitation which we represent through the localized Gaussian modelling, $\vec{R}_0$ the equilibrium position, and $\vec{e}_{\vec{\xi}}$ the vector along the [111] direction. The terms in square brackets are thus the excitation energies δE. The right hand side of equation 43 is sampled by independent runs which demands for highest accuracy. To take the limit

in 43 a functional approximation of the differences is needed which is plotted in figure 5. The center of the localized excitation has been placed at the excitation energy minimum

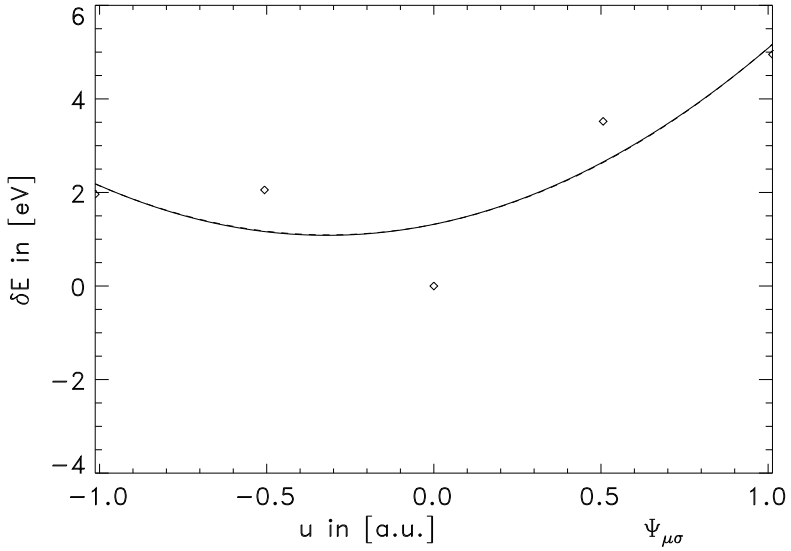

Figure 5: Excitation energy δE per electron vs. optical phonon displacement for (2,2,8) GaAs system with quadratic regression (in plot not discernible from cubic).

$\mu = 0.41$ of the undistorted crystal. This will come closer to the actual minimum, though wave function contributions from higher excitation energies cannot be excluded. The contribution from the ground state which could be highest at this point cancels because of vanishing force at equilibrium. The slope of the curve at $u = 0$ yields a value of $d = 1.45$ eV/a$_B$ per electron for the optical deformation potential. This cannot directly be compared with values of the literature because those refer to the momentum space where they also change sign. The order of magnitude seems to be realistic, however. A quantitative comparison has to include a by far larger data set of the VMC calculations. The presented results indicate that such a calculation is feasible.

4 Solid Surfaces

The scheme of QMC calculations for extended surfaces of realistic solids and its application to GaAs has been recently published. [29, 30] Former work was restricted to jellium systems. [31, 32, 33] The surface can be approximated by a cluster system which was recently applied to Si. [34]

4.1 Boundary Condition and Jellium

The geometry of a surface system breaks symmetry in surface perpendicular direction and forces new boundary conditions for which several constructions seem possible like a half-space system, a supercell, a finite cluster, or a slab of finite thickness. It is the latter we concentrate on in the subsequent analysis taking the z axis as the surface normal. The simulation cell equals the bulk one except that its periodic repetition perpendicular to the surface is cut at the surface. For instance, of an $(l \times m \times n)$ simulation cell only the l, m

part constituting Ω_0^s is repeated whereas along the normal the region is confined onto the interval $[-\frac{z_0}{2}, +\frac{z_0}{2}]$ thereby chosing for definiteness an even number n of unit cells to be enclosed in this direction. Periodic repetition with respect to Ω_0^s affects backfolding and Ewald summation again. However, the latter needs an essentially different representation. The reason is the tabulation of the two-body functions which is used again. Because of convergence, jellium parts have to be added in the separated expressions, which becomes tedious in a finite·infinite system. The infinite periodicity of Ω_0^s requires the jellium whereas the z interval makes it finite in this direction. Now the question arises where to set the confinement region. The following expression can be tabulated as a function of the difference vector

$$v^s(\vec{r}_{\gamma\gamma'}) := \sum_\nu \left(\frac{1}{|\vec{r}_\gamma - \vec{r}_{\gamma'} - \vec{R}_{||}^\nu|} + \frac{1}{\Omega}\int_\Omega \frac{-1}{|\vec{r}_\gamma - \vec{r}_{\gamma'} - \vec{R}_{||}^\nu - \vec{R}|}\, d^3R \right) - \frac{1}{|\vec{r}_{\gamma\gamma'}|}\,, \tag{44}$$

but the added jellium appearing within the parenthesis depends on the external z coordinates for a finite z integration interval $\Omega = \Omega_0^s \times [-z_0/2\,,\, +z_0/2]$. In the definition 44 the nearest neighbor term is subtracted. As a consequence of the z dependence, the electronic jellium is attached to the local electron position and the various jellium terms from electrons and ions do not locally cancel. The exact compensation must be introduced and calculated.[30] The jellium introduced in a typical interaction part according to

$$\sum_\gamma \sum_{\gamma'} Z_\gamma Z_{\gamma'} {\sum_\nu}' \left(\frac{1}{|\vec{r}_\gamma - \vec{r}_{\gamma'} - \vec{R}_{||}^\nu|} + \frac{1}{\Omega}\int_\Omega \frac{-1}{|\vec{r}_\gamma - \vec{R}_{||}^\nu - \vec{R}|}\, d^3R \right) \tag{45}$$

will cancel among electrons and ions, because it occurs $n_{el} \times (l \times m \times n)$ times in an electron summation over i and $(l \times m \times n)$ in a nuclei summation over α weighted by Z_α in equation 36. The number of electrons per unit cell is denoted as n_{el}. Here, the prime at the sum indicates that the $R_{||}^\nu = 0$ term is omitted if $\gamma = \gamma'$, i.e. no self-interaction but interaction with *all* periodic copies. The jellium integral has to be kept. To write 45 with the help of 44

$$2V_{ab} = \sum_\gamma \sum_{\gamma' \neq \gamma} \left[Z_\gamma Z_{\gamma'} \frac{1}{|\vec{r}_{\gamma\gamma'}|} \right] + \sum_\gamma \sum_{\gamma'} \left[Z_\gamma Z_{\gamma'} v^s(\vec{r}_{\gamma\gamma'}) \right] + \sum_\gamma \sum_{\gamma'} \left[Z_\gamma Z_{\gamma'} \varphi^J(z_\gamma, z_{\gamma'}) \right]. \tag{46}$$

a compensating potential of the form arises, viz.

$$\varphi^J(z_\gamma, z_{\gamma'}) := \frac{1}{\Omega}\int_{\Omega_\infty^{\gamma'} - \Omega_\infty} \frac{-1}{|\vec{r}_\gamma - \vec{r}_{\gamma'} - \vec{R}|}\, d^3R \tag{47}$$

$$\varphi^J(z_\gamma, z_{\gamma'}) = \frac{1}{\Omega}\int_{\Omega_\infty - \tilde{\Omega}_\infty^{\gamma'}} \frac{-1}{|\vec{r}_\gamma - \vec{R}|}\, d^3R\,. \tag{48}$$

The integration domain in 47 is the difference between the sets $\Omega_\infty^{\gamma'} := (\sum_\nu \Omega_\nu^s) \times [-z_0/2 - z_{\gamma'}\,,\, +z_0/2 - z_{\gamma'}]$ and $\Omega_\infty := (\sum_\nu \Omega_\nu^s) \times [-z_0/2\,,\, +z_0/2]$ where further the explicit appearance of the variable $z_{\gamma'}$ in the denominator can be shifted into the integration domain by defining $\tilde{\Omega}_\infty^{\gamma'} := (\sum_\nu \Omega_\nu^s) \times [-z_0/2 + z_{\gamma'}\,,\, +z_0/2 + z_{\gamma'}]$ in 48. The physical electrostatic analogue of the above is the potential of a dipole-like charge distribution whose solution is cited in appendix B.

The total Coulomb potential can now be written as

$$
\begin{aligned}
V_C &= \frac{1}{2}\sum_{i,j}\left[v^s(\vec{r}_{ij})\right] + \frac{1}{2}\sum_{i\neq j}\frac{1}{|\vec{r}_{ij}|} \\
&\quad - \sum_{i,\alpha}\left[Z_\alpha v^s(\vec{r}_{i\alpha})\right] - \sum_{i,\alpha}\frac{Z_\alpha}{|\vec{r}_{i\alpha}|} \\
&\quad + \frac{1}{2}\sum_{\alpha,\alpha'}\left[Z_\alpha Z_{\alpha'} v^s(\vec{r}_{\alpha\alpha'})\right] + \frac{1}{2}\sum_{\alpha\neq\alpha'}\frac{Z_\alpha Z_{\alpha'}}{|\vec{r}_{\alpha\alpha'}|} \\
&\quad + \frac{1}{2}\sum_{i,j}\varphi^J(z_i,z_j) \\
&\quad - \frac{1}{2}\sum_{i,\alpha}\left[Z_\alpha\varphi^J(z_i,z_\alpha)\right] - \frac{1}{2}\sum_{i,\alpha}\left[Z_\alpha\varphi^J(z_\alpha,z_i)\right] \\
&\quad + \sum_{\alpha,\alpha'}\left[Z_\alpha Z_{\alpha'}\varphi^J(z_\alpha,z_{\alpha'})\right] \qquad (49) \\
&= (V^s_{ee} + 2V^s_{ei} + V^s_{ii}) + (V^J_{ee} + V^J_{ei} + V^J_{ie} + V^J_{ii}) \qquad (50) \\
&=: V_s + V_J\,. \qquad (51)
\end{aligned}
$$

where the function $v^s(\vec{r})$ is calculated via a two-dimensional Ewald method the result being tabulated. In the sampling runs already performed the contribution V_J is in fact small in relation to the total energy but not negligible when comparing different geometric models of a surface. The compensation introduced here accounts for the exact vanishing of the total of jellium parts which are added for numerical convergence. This does not arise in the three-dimensional case where also a jellium is added for convergence. The possible finite size error owing to polarization is not ruled out, however.

4.2 Wave Function Ansatz for Slab

The wave function used for the slab would, on the first glance, be chosen very similar to the three-dimensional case. Of course, the parametrized single particle orbitals in the Slater determinant have to be changed at the surface to increase variational freedom accounting for relaxation and reconstruction. Also, the periodicity of the Jastrow exponent must be adapted to the remaining two-dimensional repetition, i.e. in equation 12 the two-dimensional Ewald potential $v^s(\vec{r}_{ij})$ has to be used. As it is an ansatz, we are free to use the jellium as discussed with respect to the Coulomb potential. For the kinetic energy first and second derivatives are needed presented in appendix C.

As a result, applying this wave function within the procedure presented above to the GaAs(110) surface yielded an unbounded increase of the total energy with number of atomic layers in the slab, see figure 6. Instead, the energy per atom of a surface should be limited from below by the bulk from above by the atom, according to growing stability from atom over surface to bulk. The origin of this behavior is found in the repelling nature of the Jastrow factor. As figure 7 demonstrates, the electron density expands beyond the space occupied by the ions and penetrates into the vacuum with increasing number of layers in the slab. The remedy for this failure is to improve the ansatz by adding a single particle *confinement* term $-v_{cf}(z)$ in the exponent of the Jastrow factor. The choice is rather free, its only effect should be localization of charge onto the ionic space. Thus, the

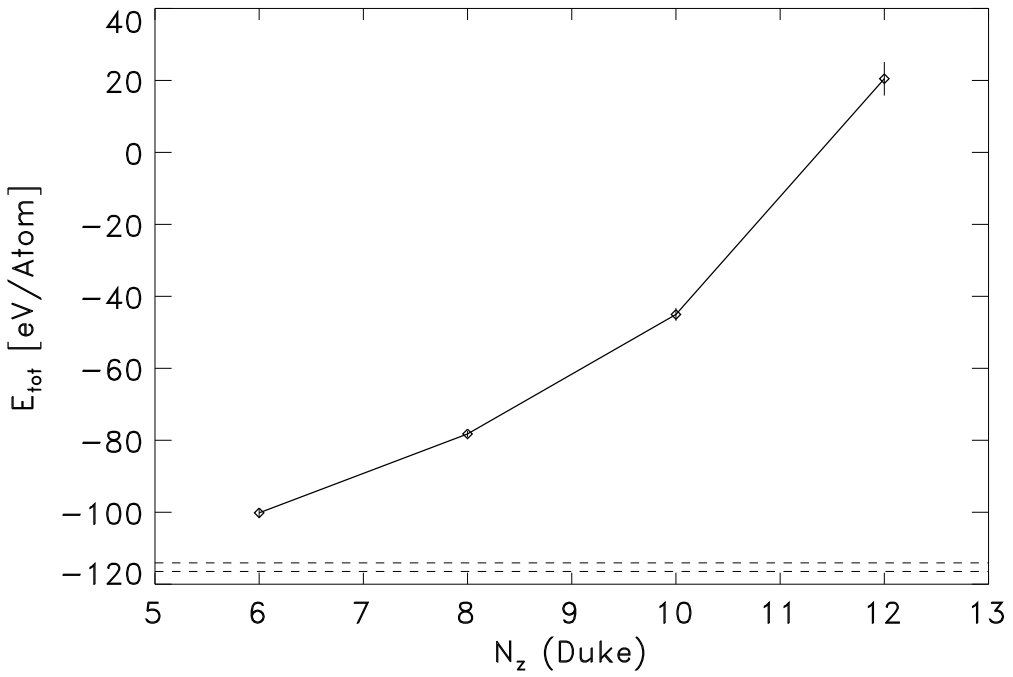

Figure 6: Total energy of GaAs(110) of Duke [35] model vs. number of layers N_Z of slab $(2, 2, N_Z)$ using nonlocal pseudopotential and unmodified Jastrow factor; broken horizontal lines represent reference energies, atom lying above bulk; slab energy moves away with increasing number of layers from expected interval between atom and bulk.

new function is chosen as

$$v_{cf}(z) = \epsilon \frac{1}{2} V_{cf} \left[\tanh\{S_{cf}(z - z_\epsilon + \epsilon\, L_{cf})\} + \epsilon \right] \tag{52}$$

with $\epsilon = +1$ (-1) for the electron at $z > 0$ $(z < 0)$ with outermost atomic planes z_{+1} (z_{-1}), resp., referring to the origin as $z = 0$. New variational parameters V_{cf}, S_{cf}, and L_{cf} arise, one of them being numerically rather redundant. The effect of this change on the optimization, the specification of the determinantal part, and the results of a total minimization procedure for the surface is presented in the next section.

4.3 Surface energy

Optimization for the GaAs(110) case according to the method described in 2.5 yields the results displayed in table 3. The correct position of the total energies of the surface between those of atom and bulk is observed. The relaxed surface has lower energy as to be expected. The values for an 8 layer slab are given for an impression of layer convergence. The comparison of the bulk energies refers to a fully three-dimensional (3D) code and the computation using the same code as for the surface but with periodic boundary also along z. The confinement of the sampled electron density using the modified Jastrow factor as displayed in figure 8, bottom plot, is clearly observed. We attribute the falling of the theoretical energy of the atom below the experimental value to an inadequacy of the pseudopotential for atomic calculations, see also end of section 3.1.

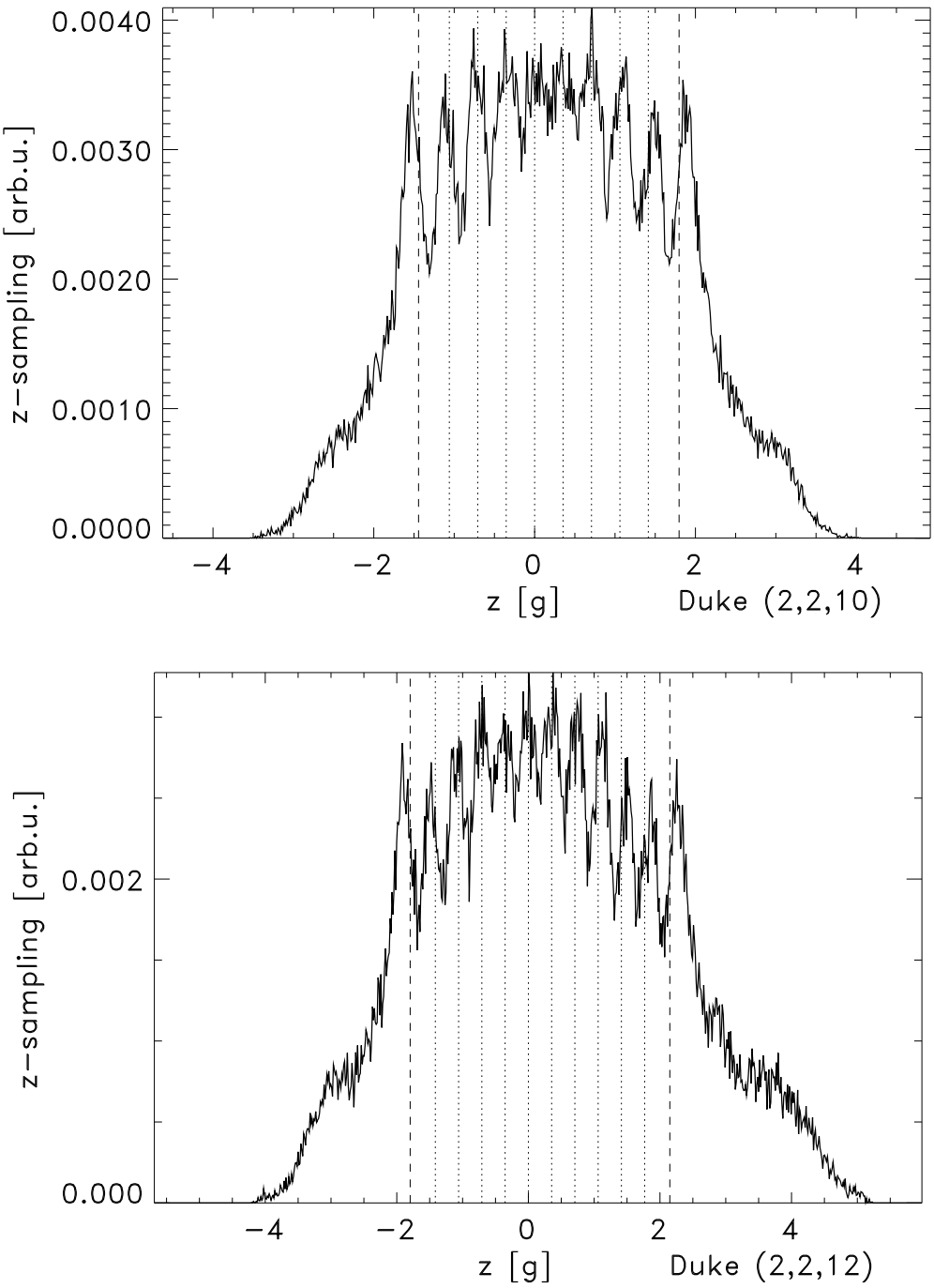

Figure 7: Electron density integrated in surface parallel direction vs. z coordinate in units of lattice constant for GaAs(110) as in fig. 6 for 10 (top) and 12 (bottom) layer slab shows artificially large space covered, nuclei planes are sketched by vertical broken lines

Note that at this stage the determinantal parameters are not yet optimized. The orbitals are centered at nuclei position as usual. However, several free parameters appear in the ansatz for the single particle wave functions suggested from physical reasons for the tetrahedrally bound compound GaAs. First, for the bulk doubly occupied hybridized orbitals are chosen by superimposing atomic s, p orbitals as e.g. obtained from

method	system	N_z	(V_{cf}, S_{cf}, L_{cf})	E [eV/atom]
Exp.	atom			-113.387
VMC	atom			-114.067 ± 0.005
VMC	ideal(110)	8	$(14.73 \pm 0.25, 0.142 \pm 0.006, 3.0)$	-115.965 ± 0.028
VMC	Duke(110)	8	$(16.08 \pm 0.19, 0.141 \pm 0.005, 3.0)$	-116.003 ± 0.030
VMC	ideal(110)	12	$(32.16 \pm 0.32, 0.104 \pm 0.001, 3.0)$	-116.238 ± 0.031
VMC	Duke(110)	12	$(33.97 \pm 0.32, 0.104 \pm 0.002, 3.0)$	-116.258 ± 0.027
VMC	2D-bulk			-116.505 ± 0.021
VMC	3D-bulk			-116.52 ± 0.04
Exp.	bulk			-116.715

Table 3: Comparison of total energies of atom, surface, and bulk for GaAs(110), with confinement parameters V_{cf}, S_{cf} optimized and L_{cf} fixed, ideal surface geometry and relaxed according to Duke with N_Z number of layers of slab.

the pseudopotential construction, viz.

$$\begin{aligned} \phi_{\alpha\mu}(\vec{r}\,) &= \phi^{\mathrm{As}}_{\alpha\mu}(\vec{r}\,) + \beta\phi^{\mathrm{Ga}}_{\tilde{\alpha}\mu}(\vec{r}\,), \\ \phi^{\mathrm{A}}_{\alpha\mu}(\vec{r}\,) &= \gamma^{\mathrm{A}}_s \phi^{\mathrm{A}}_s([\vec{r} - \vec{R}^{\mathrm{A}}_\alpha]/\zeta^{\mathrm{A}}_s) + \sum_i \tau^i_\mu \phi^{\mathrm{A}}_{p_i}([\vec{r} - \vec{R}^{\mathrm{A}}_\alpha]/\zeta^{\mathrm{A}}_p), \quad A = As, Ga\,. \end{aligned} \tag{53}$$

The index α runs over the GaAs pairs of the simulation cell, μ denotes the 4 tetrahedral directions from an Arsenic nucleus with vectors $\vec{\tau}_\mu$, and i refers to the cartesian coordinates. This leads to 4 parameters ζ for compression of the orbitals, 2 parameters for atomic hybridization, and 1 parameter for molecular hybridization. For the surface, one has to take care of the occupied As dangling bond with

$$\phi^{\mathrm{DB}}_{\alpha\mu}(\vec{r}) = \gamma^{\mathrm{As}}_s \phi^{\mathrm{As}}_s([\vec{r} - \vec{R}^{\mathrm{As}}_\alpha]/\zeta^{\mathrm{DB}}_s) + \gamma^{DB}_p \sum_i \tau^i_\mu(\vartheta^{DB}) \phi^{\mathrm{As}}_{p_i}([\vec{r} - \vec{R}^{\mathrm{As}}_\alpha]/\zeta^{\mathrm{DB}}_p)\,, \tag{54}$$

where ϑ^{DB} denotes a modified bonding angle. This adds another 4 parameters ζ^{DB}_s, ζ^{DB}_p, γ^{DB}_p, and ϑ^{DB} to the 7 bulk parameters, altogether 14 including the 3 Jastrow parameters. The optimization has been performed on a restricted space by decomposing the whole procedure into various stages. It thus may not reflect the lowest minimum obtainable by this ansatz. Among the many cuts through parameter space the dangling bond angle is of physical interest. For the 'best' angle $\vartheta = (29, 45 \pm 7, 41)^o$ a total energy of $E = -116.013 \pm 0,028$ eV/atom is found from the regression analysis, see figure 9. To determine the surface energy the values of the total energy obtained for two slab thicknesses are presented in table 4. The surface energy per unit cell (u.c.) is determined

System	V_{cf}	S_{cf}	L_{cf}	ζ_s	ζ_p	γ_p	ϑ	$\bar{E}_n$ [eV/atom]
(2,2,8)	16.077	0.1408	3.0	0.97	1.07	1.0	29.45	-116.012 $\pm$ 0.020
(2,2,12)	33.969	0.1041	3.0	0.97	1.07	1.0	29.45	-116,232 $\pm$ 0.015

Table 4: Optimal variational parameters and total energy of GaAs(110) (Duke model) for n=8 and 12 layers.

via $E_s(n) = n(E_n - E_b)$ from the total energy per atom of the bulk E_b and that of an n

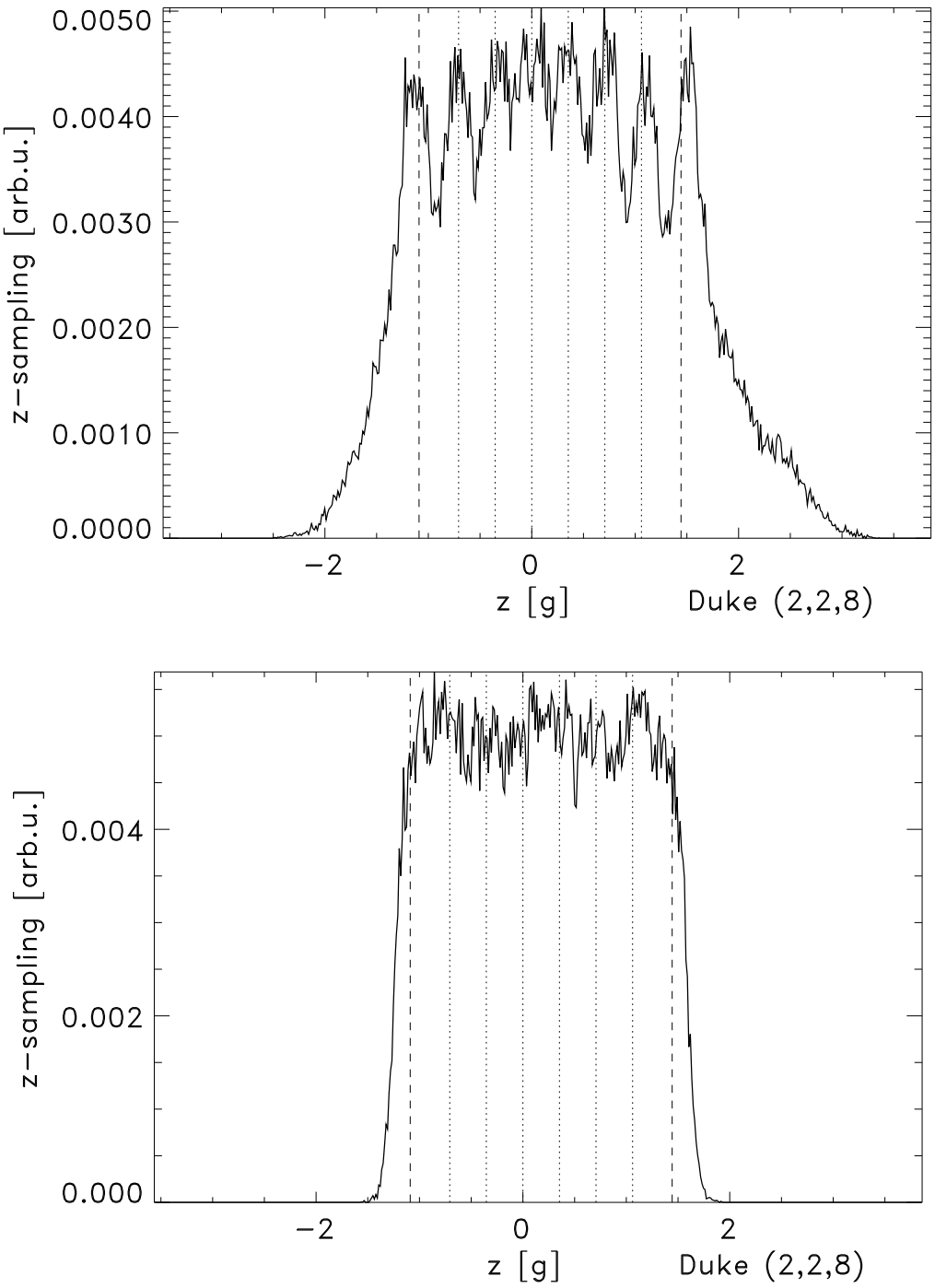

Figure 8: Electron density as in figure 7 for a (2,2,8) slab, top: without wave function confinement, bottom: with a confinement term in the Jastrow exponent.

layer surface E_n. According to both layer numbers two values for the surface energy are found [24]

$$E_s(8) \;=\; 3.94 \text{ eV/u.c.} \qquad E_s(12) = 3.28 \text{ eV/u.c.} \tag{55}$$

This has to be compared with experiment 1.21 eV [36]. In view of DFT calculations [37] which nicely reproduce the experimental value the VMC calculations above can only be

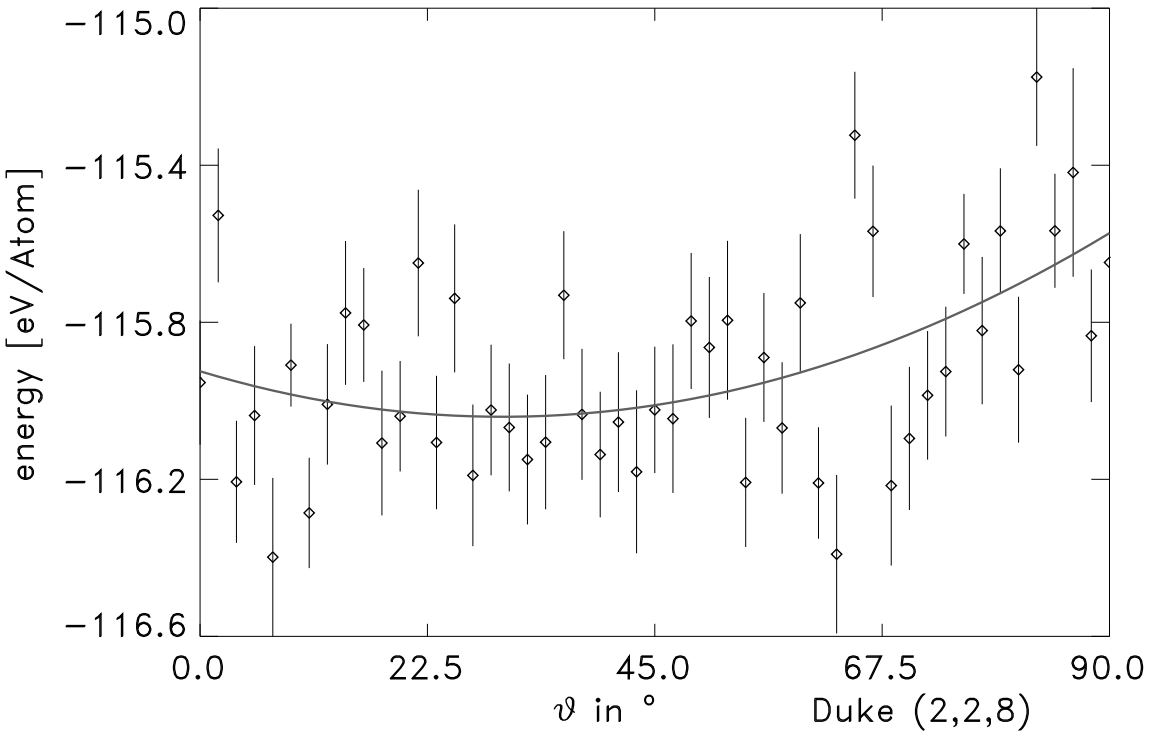

Figure 9: Total energy of GaAs(110) (Duke model) vs. dangling bond angle for a (2,2,8) slab with quadratic regression curve (solid line).

considered as a first step. The tendency the surface energy displays with the number of layers points into the correct direction. Runs with larger layer number should follow, therefore.

4.4 Surface phonons

Similar calculations as for the bulk phonons are feasible also for the surface. However, the only data available refer to the GaAs(110) surface with a displacement of the Arsenic sublattice at the surface along [001], i.e. perpendicular to the As-Ga chains, which is not an eigenmode. Thus, no comparison with experiment is possible. However, the analysis (i) shows that surface phonons can be resolved and (ii) gives an estimate of the stability of the relaxed surface in comparison to the ideal one.

In figure 10 the energy is plotted as a function of a [001] displacement of As in the interval $u \in [-0.2, +0.2] \cdot g$. Three polynomial regressions are displayed which cover increasingly a more anharmonic behavior. The curves are very similar such that by the eye alone it is difficult to decide about the value. However, it seems that the quartic regression shows an unphysical overshooting and should be probably discarded. The

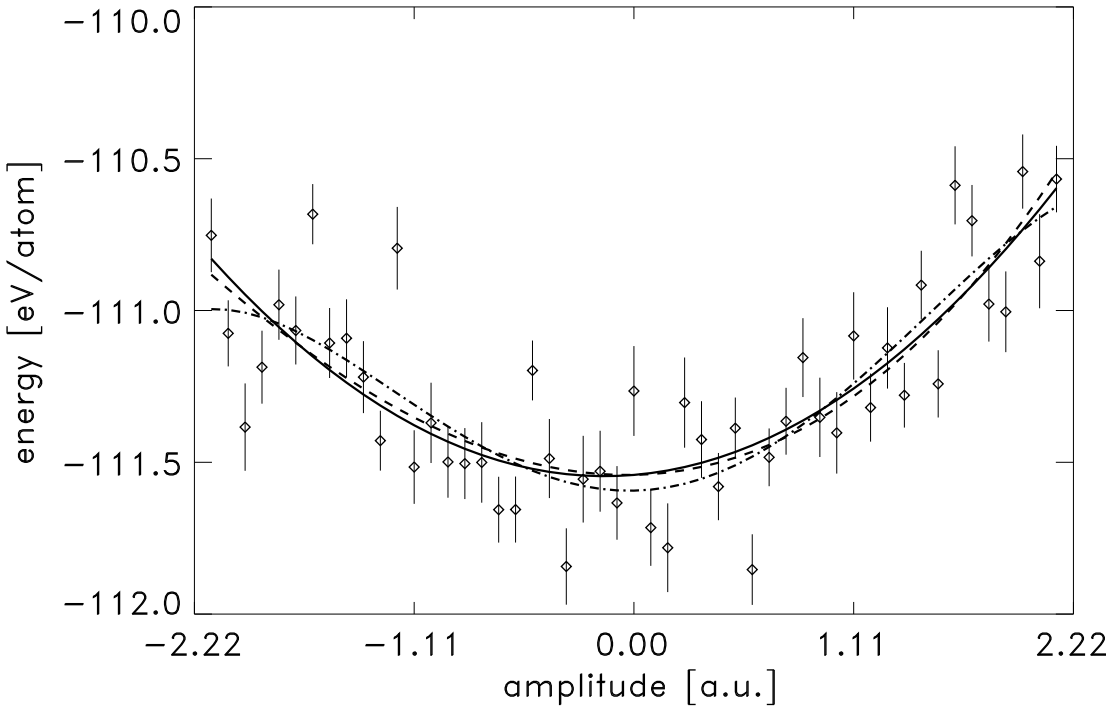

Figure 10: Total energy of GaAs(110) (Duke model) vs. amplitude of displacement of As surface sublattice along [001] for (2,2,8) system; solid, dashed, and dashed dotted line refer to quadratic, cubic, and quartic regression.

quantitative values are listed in table 5 together with those of the ideal surface. The table shows softer force constants of the relaxed surface compared to the ideal surface if the quartic fits are discarded. The equilibrium position, i.e. $u = 0$, is shifted in the ideal case showing its instability towards relaxation. The harmonic fit for the relaxed surface seems not to be adequate in view of the rather large displacements such that only the cubic curve remains which confirms roughly the stability of the relaxation according to Duke et al. [35].

model	fit	$E_{min}[eV/atom]$	$u_{min}[a.u.]$	$D[eV/a_B^2]$	$\omega[meV]$
ideal	harm.	-111,46	-0,09	6,64(22)	37,0(06)
ideal	anharm.(3.)	-111,46	-0,09	6,64(22)	37,0(07)
ideal	anharm.(4.)	-111,46	-0,09	7,2(28)	38,7(74)
Duke	harm.	-111,55	-0,17	5,80(21)	34,6(06)
Duke	anharm.(3.)	-111,54	0,00	5,80(22)	34,6(06)
Duke	anharm.(4.)	-111,59	0,00	9,3(25)	43,8(61)

Table 5: Energy minimum, position of equilibrium, force constant, and frequency for an ideal and relaxed (Duke model) surface of GaAs(110) with As sublattice displacement along [001], data taken from harmonic and anharmonic (3rd and 4th order) fits in figure 10.

5 Conclusions

The VMC method as described in this article is safely founded for ground state calculations of the bulk. For surface calculations the details have to be changed essentially, though the general scheme still fits into that of bulk solids. This concerns mainly the confinement potential and the Ewald summation with the dipole compensation. It has been shown that a surface analysis is feasible, but in view of the actually available ressources only for some prototype cases with a few parameters. Similar accuracy by similar efforts is obtained for evaluating phonon dynamics in the bulk as well as at the surface.

Acknowledgment

Support by Deutsche Forschungsgemeinschaft under contract no. Scha 360/17-1/2 is gratefully acknowledged. The numerical computations have been performed at the RZ Kiel, ZIB Berlin, and NIC Jülich.

A Polynomial decomposition and error control in optimization

The following form for the basic polynomials can be chosen

$$\begin{aligned}
p_1(\vec{\lambda}) &= 1 \\
p_2(\vec{\lambda}) &= \lambda_1 \quad \ldots \\
p_{m+1}(\vec{\lambda}) &= \lambda_m \\
p_{m+1+1}(\vec{\lambda}) &= \lambda_1^2 \quad \ldots \\
p_{m+1+m}(\vec{\lambda}) &= \lambda_m^2 \\
p_{2m+1+1}(\vec{\lambda}) &= \lambda_1\lambda_2 \\
p_{2m+1+2}(\vec{\lambda}) &= \lambda_1\lambda_3 \quad \ldots \\
p_{2m+1+m-1}(\vec{\lambda}) &= \lambda_1\lambda_m \\
p_{3m+1}(\vec{\lambda}) &= \lambda_2\lambda_3 \quad \ldots \\
p_{(m^2+3m)/2+1}(\vec{\lambda}) &= \lambda_{m-1}\lambda_m \,,
\end{aligned} \tag{56}$$

where the index at λ counts the m wave function parameters, whereas the index at the polynomials p varies from 1 to p. From the above ordering, A_0, b_i, A_{ij} in equation 30 are related to the coefficients in 29 by

$$\begin{aligned} A_0(\vec{a}) &= a_1 \\ \vec{b}(\vec{a}) &= (a_2, \ldots, a_m)^T \\ A_{ii}(\vec{a}) &= a_{m+1+i} \quad , i = 1 \ldots m \\ A_{ij}(\vec{a}) &= a_k/2 \quad , i = 1 \ldots m-1,\, j > i \quad \text{mit} \\ & \quad k = 2m + 1 + [(2m - i - 2)(i - 1)]/2 + (j - 1) \\ A_{ij}(\vec{a}) &= A_{ji}(\vec{a}) \quad , i = 2 \ldots m, j < i\,, \end{aligned} \tag{57}$$

which may be directly programmed.

The statistical error of the regression analysis for derived quantities is given by a transformation using the partial derivatives D_a

$$D_a A_0(\vec{a}) = \left(\frac{\partial A_0}{\partial a_j}\right)_j \in \Re^{1\times p} \tag{58}$$

$$D_a \vec{b}(\vec{a}) = \left(\frac{\partial b_i}{\partial a_j}\right)_{ij} \in \Re^{m\times p} \tag{59}$$

$$D_a A(\vec{a}) = \left(\frac{\partial A_{ij}}{\partial a_k}\right)_{ijk} \in \Re^{m\times m\times p}\,. \tag{60}$$

Because of 57, only a few nonvanishing terms arise. The covariance matrices for $\vec{\lambda}^*$ and E^* then result as

$$V[\vec{\lambda}^*] = (D_a\vec{\lambda}^*)\, V[\vec{a}]\, (D_a\vec{\lambda}^*)^T \in \Re^{m\times m} \tag{61}$$

$$V[E^*] = (D_a E^*)\, V[\vec{a}]\, (D_a E^*)^T \in \Re \tag{62}$$

with use of

$$D_a\vec{\lambda}^* = -A^{-1}\left[(D_a A)\,\vec{\lambda}^* + \frac{1}{2} D_a\vec{b}\right] \in \Re^{m\times p} \tag{63}$$

and

$$D_a E^* = D_a A_0 + \vec{\lambda}^{*T} D_a\vec{b} + \vec{\lambda}^{*T}(D_a A)\vec{\lambda}^* \in \Re^{1\times p}\,. \tag{64}$$

B Jellium surface dipole

The potential $\varphi_+^J(z;z')$ in equation 48 is calculated from the charge distribution of two oppositely homogenously charged plates of finite width and infinite lateral extension. Their width $d_\rho(|z'|)$ and the distance $d_0(|z'|)$ between the inner faces are determined by the second argument z', viz

$$d_\rho(|z'|) = \min\left(|z'|, z_0\right), \tag{65}$$

$$d_0(|z'|) = \left|\,|z'| - z_0\,\right|\,. \tag{66}$$

Because of the symmetry we can write

$$\varphi^J(z,z') = \begin{cases} \varphi_+^J(z;z'), & z' \geq 0 \\ \varphi_+^J(z-z';z'), & z' < 0\,. \end{cases} \tag{67}$$

with

$$\varphi_+^J(z;z') = \varphi_0 + \frac{\mathrm{sgn}(z')}{\Omega_0^s z_0} \times \tag{68}$$
$$\times \begin{cases} 0, & z \in (-\infty\,,\,-\frac{z_0}{2}] \\ \frac{1}{2}(z+\frac{z_0}{2})^2, & z \in (-\frac{z_0}{2}\,,\,-\frac{z_0}{2}+d_\rho] \\ d_\rho(z+\frac{z_0}{2}-\frac{d_\rho}{2}), & z \in (-\frac{z_0}{2}+d_\rho\,,\,-\frac{z_0}{2}+d_\rho+d_0] \\ -\frac{z^2}{2}+(-\frac{z_0}{2}+2d_\rho+d_0)(z+\frac{z_0}{2})+ & \\ \frac{1}{2}(\frac{z_0}{2})^2-d_\rho(d_\rho+d_0)-\frac{d_0^2}{2}, & z \in (-\frac{z_0}{2}+d_\rho+d_0\,,\,-\frac{z_0}{2}+2d_\rho+d_0] \\ d_\rho d_0+d_\rho^2, & z \in (-\frac{z_0}{2}+2d_\rho+d_0\,,\,+\infty)\,. \end{cases}$$

An additional constant of this potential would cancel in 49 and has been arbitrarily fixed by setting the potential to zero at $z \to -\infty$.

C Two-dimensional Ewald sum

Method and decomposition are analogous to the three-dimensional case and only the results are cited for completeness. For a description of the general method see Tosi [39]. The potential 44 obtained from summing over the two-dimensional lattice with inclusion of the jellium yields

$$\begin{aligned} v^s(\vec{r}) &= \sum_{\vec{R}_\parallel^\nu}\left(\frac{1}{|\vec{r}-\vec{R}_\parallel^\nu|}-\frac{1}{|\vec{r}+\alpha\,\mathrm{sgn}(z)\vec{e}_z-\vec{R}_\parallel^\nu|}\right)-\frac{1}{|\vec{r}\,|} \\ &+ \frac{2\pi}{\Omega_0^s}\sum_{\vec{G}_\parallel\neq 0}\frac{\exp[i\,\vec{G}_\parallel\cdot\vec{r}_\parallel-|\vec{G}_\parallel|(|z|+\alpha)]}{|\vec{G}_\parallel|} \\ &- \frac{2\pi}{\Omega_0^s}\begin{cases}\alpha, & z\notin[-\frac{z_0}{2},+\frac{z_0}{2}] \\ \alpha+|z|-\frac{1}{z_0}\left[\left(\frac{z_0}{2}\right)^2+z^2\right], & z\in[-\frac{z_0}{2},+\frac{z_0}{2}]. \end{cases} \end{aligned} \tag{69}$$

The convergence parameter $\alpha \geq 0$ is analogous to the three-dimensional case which conveniently is chosen to be z dependent. T he derivative results in

$$\begin{aligned} \vec{\nabla}v^s(\vec{r}) &= -\sum_{\vec{R}_\parallel^\nu}\left(\frac{\vec{r}-\vec{R}_\parallel^\nu}{|\vec{r}-\vec{R}_\parallel^\nu|^3}-\frac{\vec{r}+\alpha\,\mathrm{sgn}(z)\vec{e}_z-\vec{R}_\parallel^\nu}{|\vec{r}+\alpha\,\mathrm{sgn}(z)\vec{e}_z-\vec{R}_\parallel^\nu|^3}\right)+\frac{\vec{r}}{|\vec{r}\,|^3} \\ &+ \frac{2\pi}{\Omega_0^s}\sum_{\vec{G}_\parallel\neq 0}\frac{i\,\vec{G}_\parallel-|\vec{G}_\parallel|\,\mathrm{sgn}(z)\,\vec{e}_z}{|\vec{G}_\parallel|}\exp[i\,\vec{G}_\parallel\cdot\vec{r}_\parallel-|\vec{G}_\parallel|(|z|+\alpha)] \\ &- \frac{2\pi}{\Omega_0^s}\begin{cases}0\,, & z\notin[-\frac{z_0}{2},+\frac{z_0}{2}] \\ \left[\mathrm{sgn}(z)-\frac{z}{z_0/2}\right]\vec{e}_z\,, & z\in[-\frac{z_0}{2},+\frac{z_0}{2}]. \end{cases} \end{aligned} \tag{70}$$

The Laplacian is obtained by Poisson's equation which leads to

$$\Delta v^s(\vec{r}) = \frac{4\pi}{\Omega_0^s z_0}\begin{cases}0\,, & z\notin[-\frac{z_0}{2},+\frac{z_0}{2}] \\ 1\,, & z\in[-\frac{z_0}{2},+\frac{z_0}{2}]. \end{cases} \tag{71}$$

No sources at the periodically copied positions apply within the simulation cell, of course.

References

[1] W.L. McMillan, Phys. Rev. **138**, A 442 (1965)

[2] D.M. Ceperley, G.V. Chester, and M.H. Kalos, Phys. Rev. B **16**, 3081 (1977)

[3] W.M. C. Foulkes, L. Mitáš, R.J. Needs, and G. Rajagopal, Rev. Mod. Phys. **73**, 33 (2001)

[4] D.M. Ceperley und B.J. Alder, Phys. Rev. Lett. **45**, 566 (1980)

[5] S.H. Vosko, L. Wilk, and M. Nusair, Can. J. Phys. **58**, 1200 (1980)

[6] J.P. Perdew and A. Zunger, Phys. Rev. B **23**, 5048 (1981)

[7] R.Q. Hood, M.-Y. Chow, A.J. Williamson, G. Rajagopal, and R.J. Needs, Phys. Rev. B **57**, 8972 (1998)

[8] A.J. Williamson, R.Q. Hood, R.J. Needs und G. Rajagopal, Phys. Rev. B **57**, 12140 (1998)

[9] N. Metropolis, A.W. Rosenbluth, M.N. Rosenbluth, A.H. Teller, and E. Teller, J. Chem. Phys. **21**, 1087 (1953)

[10] H. Eckstein and W. Schattke, Physica A **216**, 151 (1995)

[11] S. Fahy, X.W. Wang, and S.G. Louie, Phys. Rev. B **42**, 3503 (1990)

[12] D.R. Hamann, M. Schlüter, and C. Chiang, Phys. Rev. Lett. **43**, 1494 (1979)

[13] H. Eckstein, W. Schattke, M. Reigrotzki, and R. Redmer, Phys. Rev. B **54**, 5512 (1996)

[14] S. Fahy, X.W. Wang, and S.G. Louie, Phys. Rev. Lett. **61**, 1631 (1988)

[15] C.J. Umrigar, K.G. Wilson and J.W. Wilkins, Phys. Rev. Lett. **60**, 1719 (1988)

[16] C.J. Umrigar, M.P. Nightingale, and K.J. Runge, J. Chem. Phys. **99**, 2865 (1993)

[17] M.P. Nightingale and C.J. Umrigar, *Monte Carlo Optimization of Trial Wave Functions in Quantum Mechanics and Statistical Mechanics* in Recent Advances in Quantum Monte Carlo Methods, ed. W. A. Lester, World Scientific; Singapur (1997)

[18] A.J. Williamson, S.D. Kenny, G. Rajagopal, A.J. James, R.J. Needs, L.M. Fraser, W.M. C. Foulkes, and P. Maccullum, Phys. Rev. B **53**, 9640 (1996)

[19] C.-J. Huang, C.J. Umrigar, and M.P. Nightingale, J. Chem. Phys. **107**, 3007 (1997)

[20] P.R.C. Kent, R.J. Needs, and G. Rajagopal, Phys. Rev. B **59**, 12344 (1999)

[21] G. Rajagopal, R.J. Needs, A. James, S.D. Kenny, and W.M.C. Foulkes, Phys. Rev. B **51**, 10591 (1995)

[22] J.R. Arthur, J. Phys. Chem. Solids **28**, 2257 (1967)

[23] S. Baroni, S. de Gironcoli, A. Del Corso und P. Giannozzi, Rev. Mod. Phys. **73**, 515 (2001)

[24] R. Bahnsen, PhD thesis, Kiel (2001)

[25] S. Fahy, X.W. Wang und S.G. Louie, Phys. Rev. Lett. **65**, 1478 (1990)

[26] P.R.C. Kent, R.Q. Hood, M.D. Towler, R.J. Needs und G. Rajagopal, Phys. Rev. B **57**, 15293 (1998)

[27] R.Q. Hood, M.-Y. Chou, A.J. Williamson, G. Rajagopal, R.J. Needs, and W.M.C. Foulkes, Phys.Rev. Lett. **78**, 3350 (1997)

[28] L. Mitáš, Comp. Phys. Commun. **96**, 107 (1996)

[29] R. Bahnsen, D. Schulz, W. Schattke und R. Redmer, Czech. J. Phys. **49** (11), 1519 (1999)

[30] R. Bahnsen, H. Eckstein, W. Schattke, N. Fitzer und R. Redmer, Phys. Rev. B **63**, 235415 (2001)

[31] X.-P. Li, R.J. Needs, R.M. Martin und D.M. Ceperley, Phys. Rev. B **45** (11), 6124 (1992)

[32] P.H. Acioli und D.M. Ceperley, Phys. Rev. B **54** (23), 17199 (1996)

[33] M. Nekovee und J.M. Pitarke, Comput. Phys. Commun. **137**, 123 (2001)

[34] S.B. Healy, C. Filippi, P. Kratzer, E. Penev und M. Scheffler, Phys. Rev. Lett. **87**, 016105 (2001)

[35] C.B. Duke, S.L. Richardson, A. Paton und A. Kahn, Surf. Sci. **127**, L135 (1983)

[36] C. Messmer und J.C. Bilello, J. Appl. Phys. **52**, 4623 (1981)

[37] G. Qian, R.M. Martin und D.J. Chadi, Phys. Rev. B **37**, 1303 (1988)

[38] D. Strauch und B. Dorner, J. Phys. Condens. Matter **2**, 1457 (1990)

[39] M.P. Tosi, in *Solid State Physics* eds. F. Seitz and D. Turnbull (Academic, New York) **16**, 1 (1964)